FULL PAPER

ADVANCED
FUNCTIONAL
MATERIALS
www.afm-journal.d

Check for
updates

Influence of Heavy Atom Effect on the Photophysics of Coinage Metal Carbene-Metal-Amide Emitters

*Jiale Feng, Antti-Pekka M. Reponen, Alexander S. Romanov, Mikko Linnolahti, Manfred Bochmann, Neil C. Greenham, Thomas Penfold, and Dan Credgington**

The effect of the heavy metal atom on the photophysics of carbene-metal-amide (CMA) photoemitters is explored, where the metal bridge is either Au, Ag, or Cu. Spectroscopic investigations reveal the coupling mechanism responsible for communication between the singlet and triplet manifolds. The photophysical properties do not reflect expected trends based upon the heavy atom effect, as both direct coupling between charge-transfer states and spin-vibronic coupling via a ligand-centered triplet state are present. Direct coupling is weakest for CMA(Ag), increasing the importance of the spin-vibronic pathway and rendering its properties more sensitive to inter-state energy gaps than for the Au and Cu-bridged analogues. The measured activation energy correlates with the expected exchange energy of the charge-transfer state, which is also closely related to the length of the bonds joining the carbene and amide ligands, and decreases in the order CMA(Cu) > CMA(Au) > CMA(Ag). These findings reveal that reducing interference between charge-transfer and ligand-centers excited, and minimizing exchange energy, are required for developing efficient luminescent CMA complexes.

1. Introduction

Carbene-metal-amides (CMAs) are a promising family of organometallic donor-bridge-acceptor photoemitters with potential for use in highly efficient organic light-emitting diodes. The prototype of this family[1] employs cyclic (alkyl)(amino) carbene (CAAC) acceptor and carbazole (Cz) donor bridged by a two-coordinate d^{10} coinage metal (Au, Ag, Cu) atom. Gold-bridged CMA emitters have been investigated in detail,[1–3] and all three coinage metals have been successfully demonstrated in organic LED (OLED) devices.[4–7] CMAs are characterized by particularly high rates of luminescence from triplet excited states, yet the origin of this rapid emission is not well understood. We and others have noted that the rate of emission from CMA(Ag) compounds can exceed that of heavier CMA(Au) compounds.[4,5] However, the influence of spin-orbit coupling (SOC) provided primarily by heavy bridge atom has not been explored experimentally. We have previously shown that direct SOC between singlet and triplet charge-transfer (CT) states is implicated in gold-bridged coinage metal variants,[8] in contrast with many prevailing models for SOC in organic thermally-activated delayed-fluorescence (TADF) archetypes.[9–12] However, this might be expected to change as the mass of the heavy bridging atom is reduced. Here we explore the influence of the heavy atom effect on the emission kinetics of CMAs.

We have recently shown that the charge-transfer (CT) states of gold-bridged CMAs can be shifted by around 210 meV relative to the ligand-centered locally-excited (LE) states through electrostatic interactions with host molecules in a solid matrix.[8] We use this method for tuning the CT-LE energy gap to provide a direct experimental probe of the coupling mechanism in these coinage metal-bridged CMAs.

We find that the strength of direct SOC between ^{1}CT-^{3}CT reduces in the order CMA(Cu) > CMA(Au) > CMA(Ag) as a result of both decreased d-orbital contribution to the highest occupied molecular orbital (HOMO) and lowest unoccupied molecular orbital (LUMO) and the decreased heavy atom effect. However, the spin-vibronic coupling between ^{3}CT and ^{1}CT via an intermediate ^{3}LE state does not vary significantly among the coinage metal CMAs. Spin-vibronic coupling therefore becomes more important as the direct SOC strength drops, making the photophysical properties of CMA(Ag) very sensitive to the CT-LE energy gap. In contrast, for CMA(Au) and CMA(Cu), we find that the direct SOC between CT states remains the dominant effect, with activation energies insensitive to the CT-LE gap. In all cases, we find that coupling between CT and LE

J. Feng, A.-P. M. Reponen, Prof. N. C. Greenham, Dr. D. Credgington
Cavendish Laboratory
Department of Physics
University of Cambridge
JJ Thomson Avenue, Cambridge CB3 0HE, UK
E-mail: djnc3@cam.ac.uk
Dr. A. S. Romanov, Prof. M. Bochmann
School of Chemistry
University of East Anglia
Earlham Road, Norwich NR4 7TJ, UK
Prof. M. Linnolahti
Department of Chemistry
University of Eastern Finland
Joensuu Campus, Joensuu FI-80101, Finland
Dr. T. Penfold
Chemistry
School of Natural and Environmental Sciences
Newcastle University
Newcastle upon Tyne NE1 7RU, UK

The ORCID identification number(s) for the author(s) of this article can be found under https://doi.org/10.1002/adfm.202005438.

**ADVANCED
SCIENCE NEWS**

www.advancedsciencenews.com

**ADVANCED
FUNCTIONAL
MATERIALS**

www.afm-journal.de

Figure 1. Chemical structure of coinage metal bridged carbene-metal-amide (CMA) photoemitters.

states has a detrimental effect on photoluminescence performance and should be avoided in these materials.

2. Results and Discussion

2.1. Coinage Metal Carbene-Metal-Amide Molecules

The chemical structures of coinage metal CMAs are illustrated in **Figure 1**. The HOMO and the LUMO of three CMAs are shown in Figure S1, Supporting Information. The orbital contributions to vertical excitations (S_0 to S_1–S_6) are tabulated in Table S1, Supporting Information, calculated by time dependent density functional theory (TD-DFT) utilizing the hybrid MN15 functional with the def2-TZVP basis set. The contributions from the metal atom orbitals to the electron density in the HOMO/LUMO are tabulated in Table S2, Supporting Information, and are consistent for a range of functionals. For all three CMAs, a large ground-state electrostatic dipole moment of around 15 D aligned along the carbene carbon (C)-metal (M)-amide nitrogen (N) axis is observed, arising from the electron-deficient CAAC group and the electron rich Cz group. Natural transition orbitals of the S_0 to S_1 excitation are 98% HOMO-to-LUMO. The S_1 state therefore has significant charge-transfer character, shifting electron density back from the amide to the carbene group. This reduces the electrostatic dipole moment to around 5 D and reverses its sign.[1,13] This unusually-large ground state dipole and decreased excited state dipole are critical for manipulating the CT energy and probing the coupling mechanism responsible for intersystem crossing (ISC).[8]

The calculated bond length between the carbene carbon and the amide nitrogen (C−M−N) and HOMO–LUMO overlaps differ between three metal atoms, with silver-bridged CMA possessing the longest bond (4.094 Å) and the smallest HOMO/LUMO overlap (25%), compared to 3.977 Å/36% in CMA(Au) and 3.770 Å/29% in CMA(Cu). These values are consistent for a range of functionals, and with crystallographically-determined bond lengths, as shown in Table S3, Supporting Information. This trend may be understood by considering that relativistic effects are very much stronger in Au(I) than in Ag(I), and absent in Cu(I). These lead to a contraction of the 6s and expansion of

the 5d orbitals, resulting in a stronger back-bonding component into the carbene p-orbital of CMA(Au) than for CMA(Cu) and CMA(Ag). As a result, the Au−C bond is relatively shorter than the Au−N bond, and both bonds are also anomalously small due to the lanthanide contraction, which affects the Au−C and Au−N bond lengths equally.

The steady-state absorption spectra of all three emitters in toluene show similarities as shown in Figure S2a, Supporting Information: Direct absorption to the singlet CT state at around 400 nm and ligand-centered excitations of carbene and amide groups at shorter wavelength. The oscillator strength of the CT band follows the same trend as the calculated HOMO–LUMO overlap, as might be expected, decreasing in the order CMA(Au) > CMA(Cu) > CMA(Ag). An additional effect may also arise from the larger C−M−N distance of CMA(Ag), resulting in a shallower torsional potential around the M−N bond, which makes it easier for CMA(Ag) to become distorted from the largely coplanar ground state minimum, further reducing average oscillator strength.[14] Figure S2b, Supporting Information, shows the steady-state emission peaks of CMA(Au), CMA(Ag), and CMA(Cu) in toluene are around 528, 544, and 515 nm respectively at 300 K. These are all broad unstructured spectra consistent with emission from a CT state.

2.2. Intersystem Crossing Rate of Coinage Metal Carbene-Metal-Amides in a Non-Polar Solid-State Matrix

To understand the effect of the metal on the excited state properties of the CMAs, we first measure the ISC time using transient absorption (TA) spectroscopy of dilute solid films, shown in **Figure 2**. We have previously shown that in both solid state and solution,[1,8,14] direct photoexcitation of the CT band for CMA materials populates a short-lived (ps) CT singlet state, which converts to a long-lived (ns-µs) species that shares kinetics with CT emission. We assign this long-lived species to the CT triplet, and consider the interconversion to represent ISC between CT states. Deconvolution of the TA maps reveal two dominant independent time-varying species, which are assigned to short-lived singlets and long-lived triplets. The ISC time is estimated by the crossover of singlet and triplet kinetics, and shown in Figure 2d and Figure S12, Supporting Information. The ISC times measured in this way (representing the decay half-life) are 6.0 ps for CMA(Au), 32.2 ps for CMA(Ag), and 3.7 ps for CMA(Cu). For comparison, mono-exponential fits to the singlet kinetics yield decay lifetimes of 9 ps for CMA(Au), 60 ps for CMA(Ag), and 5 ps for CMA(Cu). These solid state measurements contrast with longer ISC times for CMA(Cu) and CMA(Ag) previously reported in dilute solution.[14] Note that in the solid state, ISC is constrained to occur close to the photoexcited ground-state geometry, for which a coplanar arrangement of the donor and acceptor is preferred, while in solution, ISC occurs during or after relaxation toward the relaxed S_1 geometry (donor and acceptor close to orthogonal).[14,15] The trend and timescales in dilute solid state are consistent with recent computational results which demonstrated that the rate of ISC for CMA(Ag) is the slowest, as SOC between the ^{1}CT-^{3}CT states was smallest at 2.58 cm^{-1}.[14] Moreover, the rapid ISC predicted
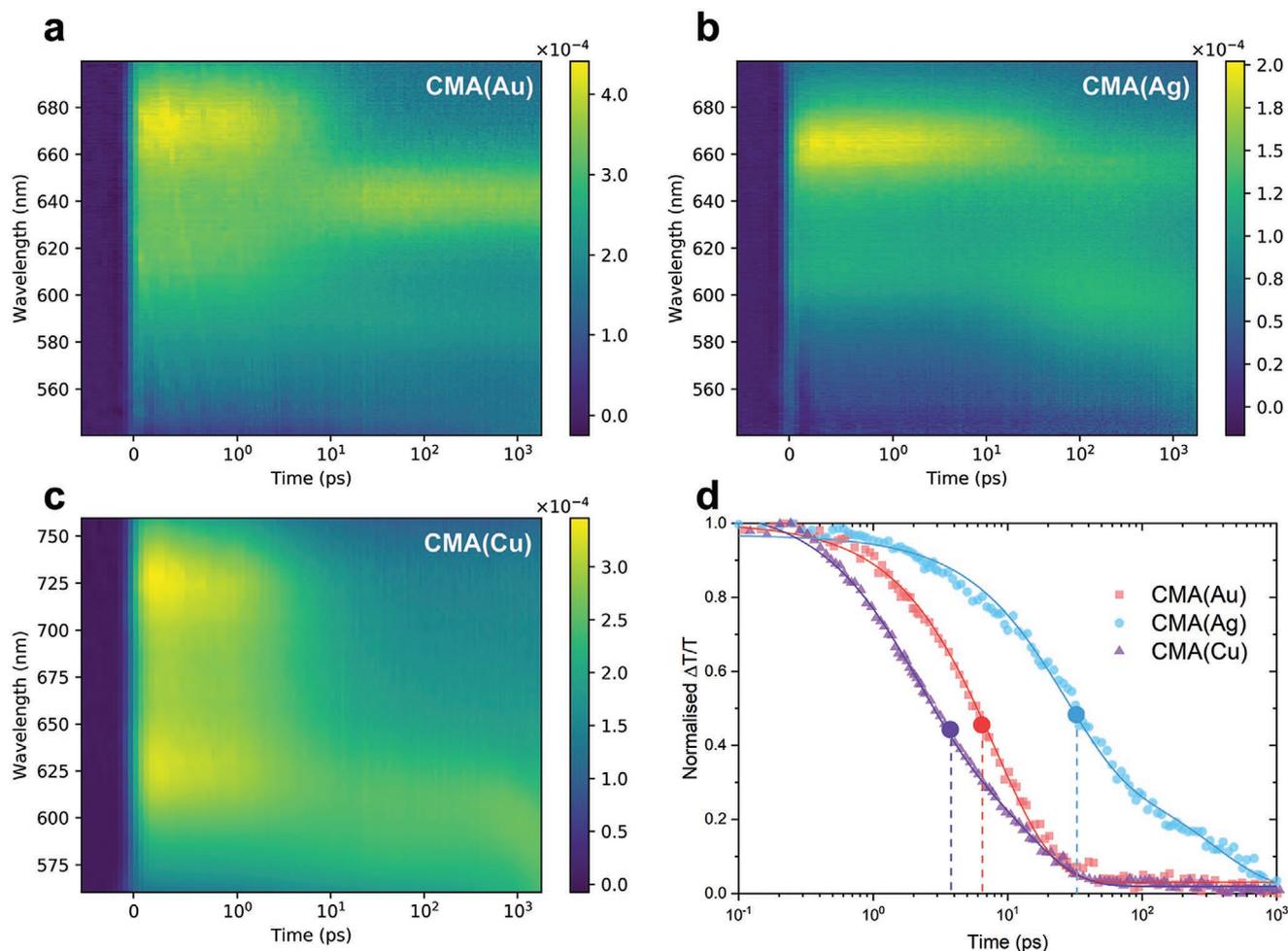
Figure 2. Room temperature transient absorption spectra of a) 5 wt% CMA(Au) in PS thin film, b) 5 wt% CMA(Ag) in PS thin film, and c) 5 wt% CMA(Cu) in PS thin film on picosecond-nanosecond time scales. The intensity is shown in $\Delta T/T$, the fractional change in transmission. Samples were pumped at 400 nm under 50 μW pump power. d) The normalized deconvoluted singlet kinetics of CMA(Au), CMA(Ag), and CMA(Cu) are presented. The intersystem crossing time of each sample is estimated by the crossover of singlet and triplet kinetics labelled by spots, around 6.0 ps for CMA(Au), 32.2. ps for CMA(Ag), and 3.7 ps for CMA(Cu). Solid lines are a guide to the eye. The triplet growth kinetics are not included for clarity. Full kinetics are shown in Figure S12, Supporting Information. Spectral deconvolution is achieved by isolating covarying regions of the TA spectra by iterative application of a genetic algorithm (GA). The full details of this approach is described in literature.[16,17] Singular value decomposition of the TA maps reveal two dominant components. As such, the genetic algorithm was restricted to find two independent time-varying species. Manual extraction of crossover time, considering kinetics only at the absorption peaks of the early and late time species, yields approximately the same results.

for CMA(Cu) when compared with the other coinage metal bridges in a similar environment is likewise reproduced.

2.3. Photophysical Characterizations of Coinage Metal Carbene-Metal-Amides in a Non-Polar Solid-State Matrix

We first examine doping the emitters in polystyrene (PS), which is considered an electronically and electrostatically inert matrix for photophysical investigations,[18] and therefore will not exert a strong influence on the CMA emitters or shift the CT state energy. **Figures** 3a,4a and Figure S3, Supporting Information, present the steady-state absorption and photoluminescence (PL) spectra of CMA(Cu), CMA(Ag), and CMA(Au) doped into PS host at concentrations from 100% (neat film) to 5% by weight. PL spectra gradually blueshift on dilution, by around 70 meV

for CMA(Au), 75 meV for CMA(Cu), and 87 meV for CMA(Ag). We interpret this arising from dilution limiting diffusional relaxation through the disordered density of states (DOS), as previously observed.[8] The luminescence lifetime of coinage metal CMAs remains relatively constant against concentration in host, with CMA(Ag) the fastest (0.65 μs), CMA(Cu) the slowest (2.6 μs), and CMA(Au) in between (1.0 μs), see Figures 3b,4b and Figure S4, Supporting Information. Lifetimes at all concentrations are tabulated in Table S4, Supporting Information. Note that the dependence of these luminescence lifetimes on bridge atomic number contrasts with that of the ISC times measured using TA. The luminescence rate of all three CMAs in PS is strongly temperature dependent. The cryogenic steady-state PL of CMA(Cu) and CMA(Au) remains unstructured see Figure 3d and Figure S5, Supporting Information. We interpret this as indicating that in PS matrix, PL primarily

**ADVANCED
SCIENCE NEWS**

www.advancedsciencenews.com

**ADVANCED
FUNCTIONAL
MATERIALS**

www.afm-journal.de
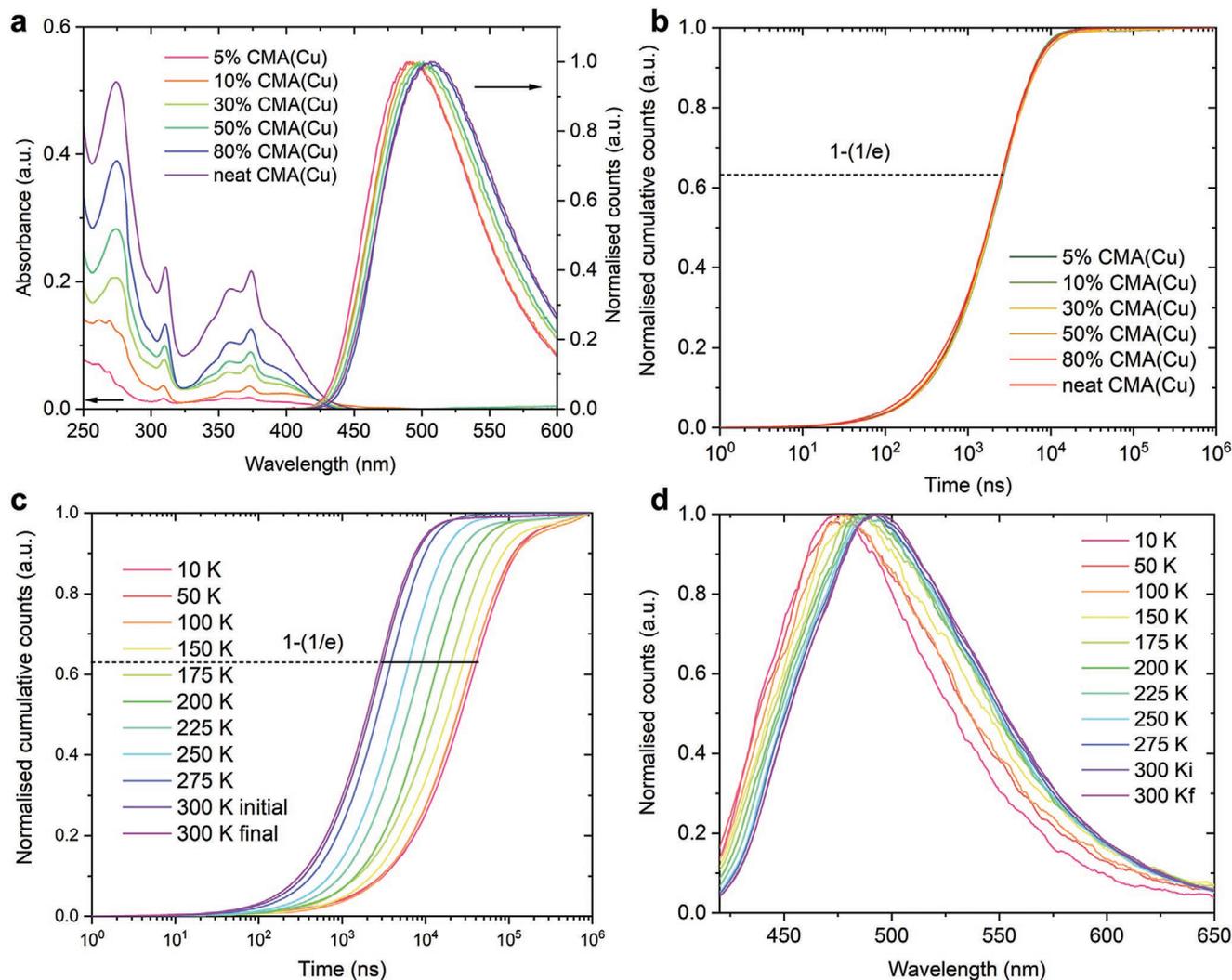
Figure 3. a) Steady-state absorption and photoluminescence of CMA(Cu) in PS host at different concentrations. b) Room temperature emission integral of CMA(Cu) in PS composites, with 1-(1/e) labelled as the characteristic luminescence lifetime. c) Cryogenic emission integral of 10% CMA(Cu) in PS with 1-(1/e) labelled as the characteristic luminescence lifetime. "Initial" data taken at 300 K before cooling the film to 10 K, "Final" data upon warming back to 300 K after low-temperature measurements. d) Temperature dependent steady-state photoluminescence of 10% CMA(Cu) in PS.

arises from CT emission for these compounds at all temperatures. The only difference upon cooling is a slight blueshift in the steady-state PL, which we interpret as due to the restriction of triplet diffusion at low temperature.[8] The luminescence lifetime increases by a factor of 50 for CMA(Au)[8] and 15 for CMA(Cu) at 10 K compared to 300 K. The thermal activation energy extracted from the temperature dependent PL decay rate is of CT emission for CMA(Cu) around 103 meV and CMA(Au) around 75 meV in PS.[8]

By contrast, for the silver-bridged CMA, shown in Figure 4c,d, the emission spectrum transforms below 150 K and structured emission consistent with triplets localized on the carbazole ligand (^{3}LE(Cz), shown in Figure S6, Supporting Information) appears and begins to compete with the unstructured CT emission in the steady-state PL. This drastically increases the luminescence lifetime, by a factor of 700 at 10 K compared to 300 K, as ^{3}LE(Cz) is only very weakly dipole coupled to the electronic ground state.

2.4. Photophysical Characterizations of Coinage Metal Carbene-Metal-Amides in the Presence of Strong Solid-State Electrostatic Interactions

We have previously shown that strong electrostatic interactions between the CMA emitters and polar host molecules are able to increase CT state energies relative to the triplets localized to the carbazole donor ^{3}LE(Cz).[8] The small-molecule host diphenyl-4-triphenylsilyl-phenyl-phosphine oxide (TSPO1) with a large permanent electric dipole moment of 4.1 D is a suitable candidate.[8] Steady-state absorption and photoluminescence spectra of CMA(Cu), CMA(Ag), and CMA(Au) in TSPO1 host at various concentrations are shown in **Figures 5**a,**6**a and Figure S7, Supporting Information, where large PL blueshift is observed: 134, 161, and 210 meV for Cu, Ag, and Au bridged-CMA respectively when decreasing the doping concentration from neat films to 5 wt% CMA:TSPO1 composite films. We interpret this as the additional influence of increased solid-state
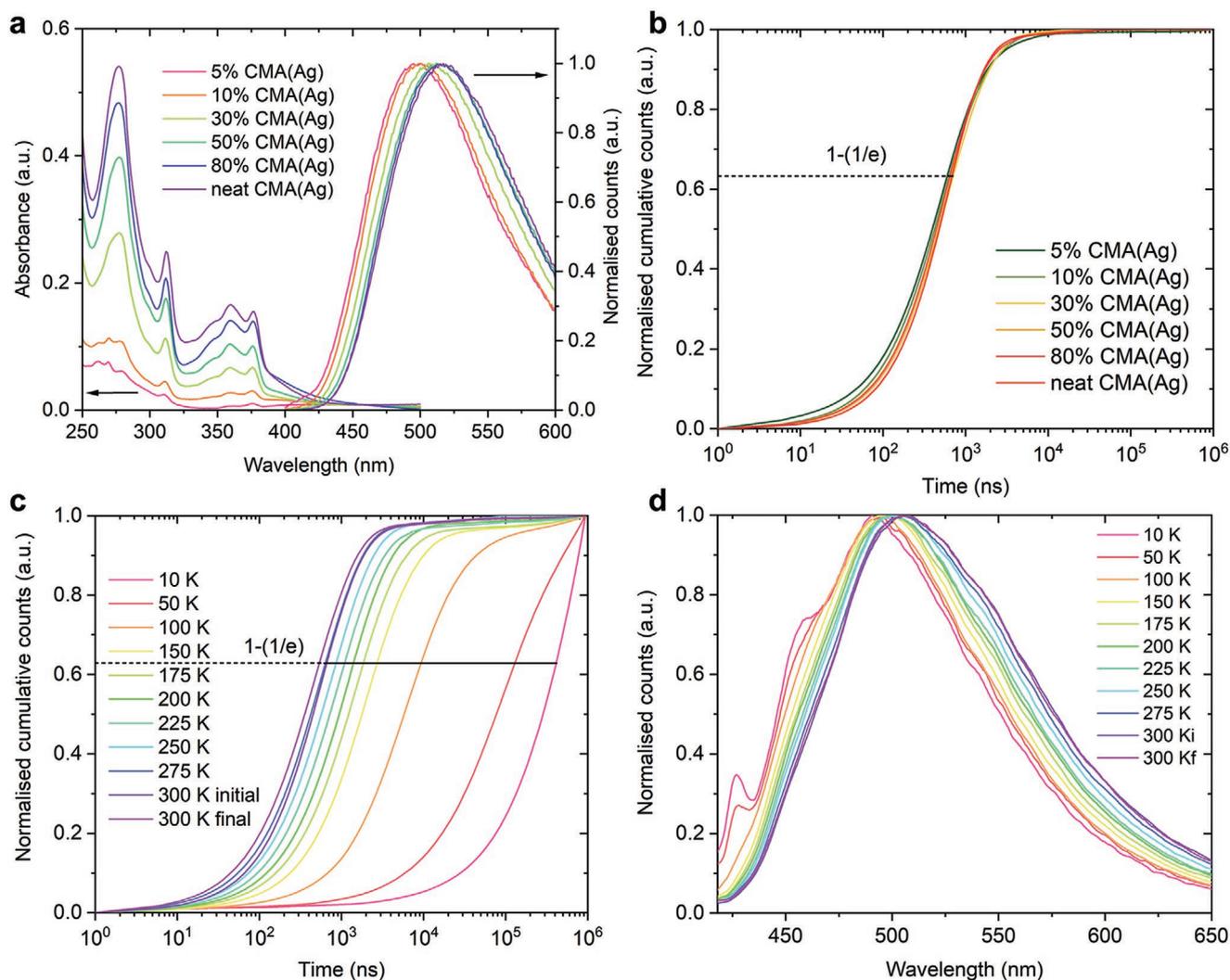
Figure 4. a) Steady-state absorption and photoluminescence of CMA(Ag) in PS host at different concentrations. b) Room temperature emission integral of CMA(Ag) in PS composites, with 1-(1/e) labelled as the characteristic luminescence lifetime. c) Cryogenic emission integral of 10% CMA(Ag) in PS with 1-(1/e) labelled as the characteristic luminescence lifetime. "Initial" data taken at 300 K before cooling the film to 10 K, "Final" data upon warming back to 300 K after low-temperature measurements. d) Temperature dependent steady-state photoluminescence of 10% CMA(Ag) in PS.

solvation in the polar host, as host fraction is increased.[8,19,20] Note that since the dipole moments of the ground and excited states are in opposition for CMA complexes, this manifests as a "negative" solid-state solvatochromism. In contrast to the behavior in PS, the luminescence lifetime increases 2.4 times for CMA(Cu) from 2.5 µs (neat film) to 6.1 µs (5%), 7.6 times for CMA(Ag) from 0.59 µs (neat film) to 4.5 µs (5%), and 1.4 times for CMA(Au) from 0.97 µs (neat film) to 1.4 µs (5%), see Figures 5b,6b and Figure S8, Supporting Information. These values are tabulated in Table S5, Supporting Information.

Figure 5c shows the time-resolved emission peak position of CMA(Cu) in TSPO1 as a function of concentration, where the redshift is due to the energy relaxation via triplet diffusion within the CT DOS, similar to that previously observed for CMA(Au).[8] By contrast, the emission peak position of CMA(Ag) blueshifts with time at doping concentrations below 50 wt%, see Figure 6c. We reason that higher energy ^{3}CT states in the DOS are closer in energy to the ^{3}LE(Cz). Mixing between

the CT and ^{3}LE(Cz) prolongs the overall luminescence lifetime, since the emission rate from the ^{3}LE(Cz) state is much lower than that of the CT state. The ^{3}CT DOS is energetically broad, and since lower-energy CT triplets mix less with ^{3}LE(Cz), they are observed to emit at earlier times. This admixed PL becomes more revealing at low temperature due to the thermally-activated nature of CT emission.

Low-temperature luminescence lifetime of 10% CMA(Cu) in TSPO1 increases by approximately a factor of 7.3, from 6.4 µs at 300 K to 47 µs at 10 K, see Figure 5d. Low-temperature steady-state PL shows that the photoluminescence is still predominantly of CT character above 150 K, but below this, structured features begin to emerge, as shown in Figure 5e. The activation energies extracted from the PL decay rate of 10% and 80% CMA(Cu) in TSPO1 host are 103.4 and 105.1 meV, which are in good agreement with value of 102.5 meV yielded from 10% CMA(Cu) in PS, see Figure 5f. However, activation energies yielded from the integrated PL intensity against temperature

**ADVANCED
SCIENCE NEWS**

www.advancedsciencenews.com

**ADVANCED
FUNCTIONAL
MATERIALS**

www.afm-journal.de
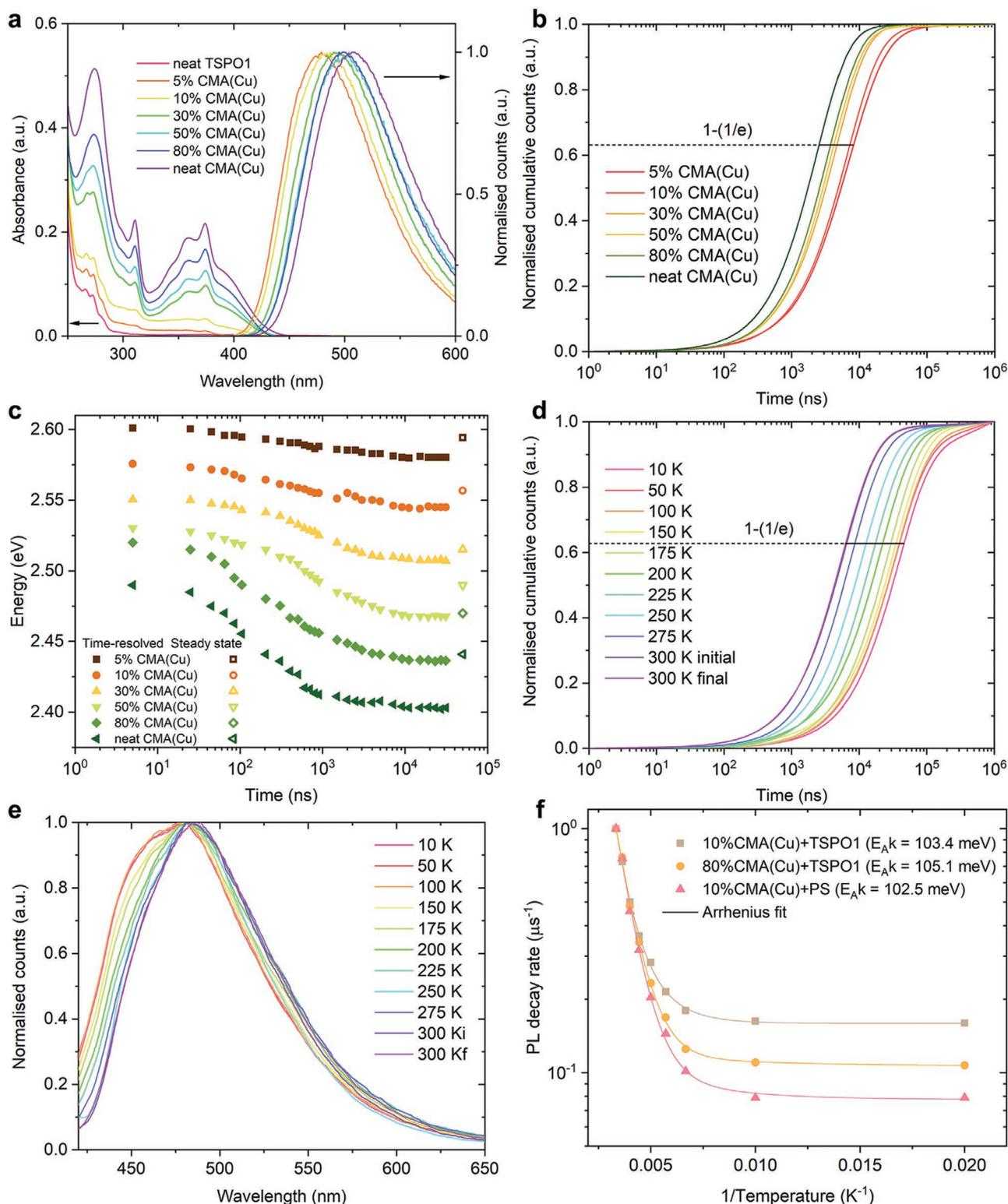
Figure 5. a) Steady-state absorption and photoluminescence of CMA(Cu) in TSPO1 host at different concentrations. b) Room temperature emission integral of CMA(Cu) in TSPO1 composites, with 1-(1/e) labelled as the characteristic luminescence lifetime. c) Room temperature time-resolved PL peak energy of CMA(Cu) in TSPO1 at different concentrations to track the spectral diffusion. d) Cryogenic emission integral of 10% CMA(Cu) in TSPO1 with 1-(1/e) labelled as the characteristic luminescence lifetime. "Initial" data taken at 300 K before cooling the film to 10 K, "Final" data upon warming back to 300 K after low-temperature measurements. e) Temperature dependent steady-state photoluminescence of 10% CMA(Cu) in TSPO1. f) PL decay rate of 10% and 80% concentration of CMA(Cu) in TSPO1 and 10% in PS at different temperatures as a function of 1/temperature. PL decay rate is the reciprocal of characteristic luminescence lifetime from cryogenic emission integral. The activation energies $E_A k$ are yielded from the Arrhenius fit.

**ADVANCED
SCIENCE NEWS**

www.advancedsciencenews.com

**ADVANCED
FUNCTIONAL
MATERIALS**

www.afm-journal.de
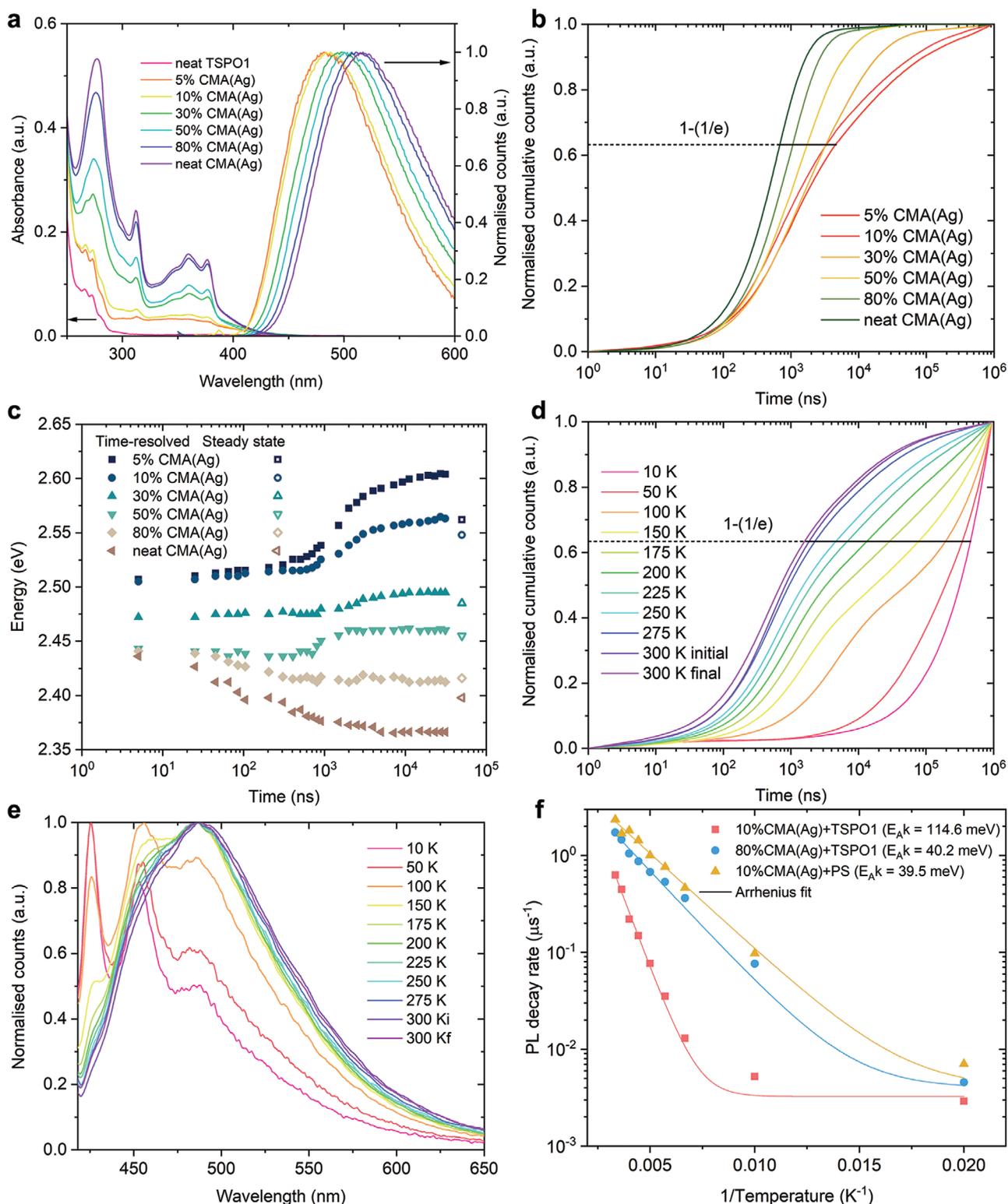
Figure 6. a) Steady-state absorption and photoluminescence of CMA(Ag) in TSPO1 host at different concentrations. b) Room temperature emission integral of CMA(Ag) in TSPO1 composites, with 1-(1/e) labelled as the characteristic luminescence lifetime. c) Room temperature time-resolved PL peak energy of CMA(Ag) in TSPO1 at different concentrations to track the spectral diffusion. d) Cryogenic emission integral of 10% CMA(Ag) in TSPO1 with 1-(1/e) labelled as the characteristic luminescence lifetime. "Initial" data taken at 300 K before cooling the film to 10 K, "Final" data upon warming back to 300 K after low-temperature measurements. e) Temperature dependent steady-state photoluminescence of 10% CMA(Ag) in TSPO1. f) PL decay rate of 10% and 80% concentration of CMA(Ag) in TSPO1 and 10% in PS at different temperatures as a function of 1/temperature. PL decay rate is the reciprocal of characteristic luminescence lifetime from cryogenic emission integral. The activation energies E_Ak are yielded from the Arrhenius fit.

**ADVANCED
SCIENCE NEWS**
www.advancedsciencenews.com

**ADVANCED
FUNCTIONAL
MATERIALS**
www.afm-journal.de

are lower than those from the PL decay rate: 70.0 meV (10% CMA(Cu) in TSPO1), 65.8 meV (80% CMA(Cu) in TSPO1), and 74.9 meV (10% CMA(Cu) in PS), see Figure S10, Supporting Information. The key difference between the two measurements is that the former incorporates non-radiative decay processes, indicating that the non-radiative decay rate in CMA(Cu) has a significant thermally activated component. This contrasts with CMA(Au),[8] and is consistent with typically lower photoluminescence quantum efficiency for CMA(Cu) measured at ambient temperature ($\approx$70%).[1,21] However, activation energy does not change with the ^{3}CT-^{3}LE(Cz) energy gap, and we thus infer that ^{3}LE(Cz) is not significantly involved in the ISC in CMA(Cu).

At low temperature, the luminescence lifetime of 10% CMA(Ag) in TSPO1 increases by a factor of 275, from 1.7 µs at 300 K to 467 µs at 10 K, see Figure 6d. Low-temperature steady-state PL shows a distinct transition from mainly unstructured CT emission to emission dominated by the structured features from the ^{3}LE(Cz) state (shown in Figure S6, Supporting Information) below 150 K, see Figure 6e. This transforms the shape of the integrated emission at low temperature. The emission spectra evolve significantly over time, with unstructured CT emission on ns timescales, and long-lived, ^{3}LE(Cz) emission, peaking at higher-energy, on µs timescales. Spectral evolution over time for 10% CMA(Ag) in TSPO1 at 10 K is shown in Figure S11, Supporting Information. In contrast to CMA(Au) and CMA(Cu), the activation energies yielded from the PL decay rate for CMA(Ag) are dependent on the ^{3}CT-^{3}LE(Cz) energy gap: 39.5 meV for 10% CMA(Ag) in PS, 40.2 meV for 80% CMA(Ag) in TSPO1, and 114.6 meV for 10% CMA(Ag) in TSPO1, see Figure 6f. While we consider the former two measurements to represent the thermal activation in the absence of significant interference from a nearby ^{3}LE(Cz) state, consistent with other reports,[4] the latter measurement represents a regime with strong interference between CT and ^{3}LE(Cz) states. For CMA(Ag), the integrated PL intensity does not show a simple thermally-activated growth, which indicates that non-radiative decay in CMA(Ag) is significantly thermally activated. This is consistent with the lower photoluminescence quantum efficiency and electroluminescence quantum efficiency reported for Ag compounds, at around 74% (PLQE) and 14% (EQE) compared to Au analogues at around 98% (PLQE) and 26% (EQE).[1,5]

2.5. Discussion of the Luminescence Mechanism of the Coinage Metal Carbene-Metal-Amides

In the previous sections, we have presented the effect of the bridging metal and host molecules on the excited state properties of CMA complexes. We find that ISC and triplet harvesting rates do not follow the trend expected for the heavy atom effect. The ISC rate is quantitively consistent with the quantum dynamics simulations of Penfold et al.[14] with a trend of CMA(Cu) > CMA(Au) > CMA(Ag) observed. CMA(Cu) exhibits a higher rate than CMA(Au) due to its stronger direct ^{1}CT-^{3}CT coupling, resulting from the larger contribution from copper d-orbitals to the lowest lying CT excited states in CMA(Cu) (Table S2, Supporting Information). The spin-orbit coupling

matrix elements (SOCMEs) are dominated by an internal effect concerning the character of the states involved in the transition, as captured in El-Sayed's rule,[22] rather than the external heavy atom effect.[14,15,23,24] CMA(Ag) has the smallest SOCME of 2.58 cm^{-1} because the silver d-orbitals mix weakly to the lowest lying CT states, similar to Au, and the smaller external heavy atom effect of Ag further reduces the size of the SOCMEs.[14] Given the weak coupling between its CT states, recent work suggests that in order to achieve effective ISC in CMA(Ag), second-order coupling to an intermediate state localized to the donor or acceptor ligands ("LE" states) may be preferred.[14]

For each CMA material, electrostatic interactions with the host are shown to blueshift the CT states. However, the LE states are relatively insensitive to such electrostatic interactions, leading to variation in the CT-LE energy gap. In principle, while both the ^{3}LE(CAAC) and ^{3}LE(Cz)[14] states may participate in the photophysics, the former appears energetically inaccessible in practice, and where ^{3}LE emission is observed (for example for CMA(Ag) hosted in TSPO1), it arises from ^{3}LE(Cz). The activation energy we measure is consistent for all CT states for CMA(Au) and CMA(Cu), and for CMA(Ag) under conditions where ^{3}LE(Cz) emission is not observed, indicating limited involvement of the LE states. We therefore consider that the emission process, which we take to be analogous with organic TADF, requires thermally-assisted mixing of ^{3}CT with ^{1}CT.[25,26] We interpret the activation energies measured herein to correspond to the energy barrier for this process. CMA(Cu) exhibits the highest energy barrier, of $\approx$100 meV, CMA(Au) an intermediate barrier ($\approx$70 meV) and CMA(Ag) the lowest energy barrier ($\approx$40 meV). These energy scales correspond to the value ΔE_{ST} commonly reported in organic TADF literature.[25,27–29] However, where ^{3}CT and ^{3}LE(Cz) are in close proximity, the nature of the energy barrier changes and its height increases, and we interpret this as the energy required to escape a local ^{3}LE(Cz) state and access states in the ^{3}CT manifold. This is similar in concept to the type-III TADF model described in the current literature,[9,12] but with the important caveat that it is ^{1}CT-^{3}CT coupling which provides the luminescence pathway. The interference from the ^{3}LE(Cz) state significantly increases the luminescence lifetime of CMA(Ag), whereas for CMA(Au) and CMA(Cu) where the direct coupling between CT states is strong, we find that the parasitic ^{3}LE(Cz) state does not significantly impact luminescence lifetime in most circumstances.

For all compounds, ISC occurs on the picosecond timescale and is therefore not a rate-limiting step for emission; indeed there is little correlation between the ISC and luminescence rates. Instead, our data supports the hypothesis that it is access to molecular configurations that permit mixing of ^{1}CT and ^{3}CT which represents the rate limiting step. Accessing such configurations is easier in CMA(Ag), owing to its flatter ground and excited state potential along torsional degrees of freedom[14] allowing the highest radiative rates. While most obviously relevant in liquid phase, in amorphous solid state we would also anticipate a broader range of both static and dynamic conformational disorder for CMA(Ag). By contrast, despite showing stronger SOC, CMA(Cu) shows low radiative rates due to its higher activation energy. The correlation between C–M–N bond length and activation energy, with the former influencing HOMO–LUMO overlap, suggests that activation energy is

closely related to the exchange energy of the CT state. Longer, more flexible, bonds, may also play a part in allowing easier reorganization, though may also contribute to nonradiative decay. The activation energy therefore represents the energy of an internal reorganization of the CT state, for instance by altering its symmetry, and in most cases, it does not represent the energy needed to access a discrete state of different quantum mechanical character, such as a ^{3}LE state.

3. Conclusions

In conclusion, we have investigated the heavy atom effect on the coinage-metal bridged CMAs to reveal its influence on the ISC and luminescence mechanism. We find that the photophysical properties do not reflect expected trends based upon the heavy atom effect, as both direct (^{1}CT-^{3}CT) coupling and spin-vibronic coupling via a local triplet state ^{3}LE(Cz) are present. The combination of the small contribution from the Ag d-orbitals to the lowest-lying CT states and lighter atom renders the weakest direct ^{1}CT-^{3}CT coupling for CMA(Ag) and thus the slowest ISC rate, making the spin-vibronic coupling more important and the photophysical properties more sensitive to the CT-LE energy gap than the Au and Cu-bridged analogues. The activation energy measured from photoluminescence spectroscopy stays relatively constant for all CT states for CMA(Au), CMA(Cu), and for CMA(Ag) where ^{3}LE(Cz) is not significantly involved. We consider that the activation energy represents the thermal energy required for mixing the ^{3}CT and ^{1}CT states to achieve luminescence. However, where the CT-LE gap is diminished, strong interference from ^{3}LE(Cz) state makes the spin-vibronic coupling dominant in CMA(Ag) and significantly reduces the emission rate.

The development of CMA complexes for high efficiency OLEDs, which rely on high radiative decay rates and high luminescence quantum efficiency, therefore requires the removal of parasitic local triplet states close to the CT energy and the minimization of exchange energy. In this respect, the design rules for such a compound echo those initially developed for organic TADF compounds, before the concept of beneficial spin-vibronic coupling between states of different character was introduced as an appropriate model.

4. Experimental Section

Synthesis of Carbene Metal Amides: Carbene metal amides were synthesized as previously reported.[1,5,21]

Sample Preparation: Host-guest thin films of different weight ratios were made from chlorobenzene solution in 20 mg mL^{-1} concentration. These well-mixed solutions were spun inside a nitrogen filled glove box onto pre-cleaned fused quartz (spectrosil) substrates at 1200 r.p.m. for 40 s at room temperature to form thin films. Samples were stored in a nitrogen glovebox to minimize degradation. Solution samples of various solvents were prepared as 1 mg mL^{-1} in the nitrogen glovebox, deoxygenated and sealed in 1-mm path length and QS-grade quartz cuvettes.

UV–vis–NIR Spectrophotometer: A Shimadzu UV-3600 Plus spectrophotometer was used to measure the steady-state absorbance of samples, which comprises three detectors: a PMT (photomultiplier tube) for the ultraviolet and visible regions and InGaAs and cooled PbS

detectors for the near-infrared region. The detectable wavelength range is between 185 and 3300 nm with resolution of 0.1 nm.

Photoluminescence Spectrometer: An Edinburgh Instruments FLS980 spectrofluorimeter was used to measure steady-state luminescence spectra. A R928P PMT detector was used in this experiment, with a wavelength range of 200 to 870 nm and a dark count rate of <50 cps (at −20 °C). The detector is operated in single photon counting mode. The PL spectra of CMA1 were collected from 350 to 650 nm with the resolution of 1 nm. Samples were excited by a 450 W Xe1 xenon arc lamp. The light from the xenon arc is focused into the monochromators by using an off-axis ellipsoidal mirror.

Temperature-Dependent ns-µs Time-Resolved Photoluminescence Measurements: Time-resolved photoluminescence spectra were measured by an electrically-gated intensified CCD (ICCD) camera (Andor iStar DH740 CCI-010) connected to a calibrated grating spectrometer (Andor SR303i). Samples were photoexcited by femtosecond laser pulses which were created by second harmonic generation in a ß-barium borate crystal from the fundamental source (wavelength = 800 nm, pulse width = 80 fs) of a Ti: Sapphire laser system (Spectra-Physics Solstice), at a repetition rate of 1kHz. The photons from the laser pulses had a wavelength of 400 nm. A 425 nm long-pass filter was used to prevent scattered laser signal from entering the camera. Temporal evolution of the PL emission was recorded by stepping the ICCD gate delay with respect to the trigger pulse. The minimum gate width of the ICCD was 5 ns. Cryogenic measurements were carried out using an Oxford Instruments Optistat continuous flow cryostat with liquid helium coolant, and an ITC 502 S temperature control unit. The 1 kHz repetition rate of the laser used in this experiment precludes accurate measure of lifetimes beyond 1 ms.

For non-exponential luminescence decays in the solid state, a characteristic lifetime rather than monoexponential decay time was quoted. The time taken to reach 63% (1-(1/e)) of the total emission integrated from 0 to 950 µs was chosen. This allowed direct comparison to lifetimes extracted from monoexponential decays.

Transient Absorption Spectroscopy: Films were drop-cast from solution, 60 µL per film on 13 mm quartz discs heated to 70 °C. Solutions of CMAs and PS in chlorobenzene were made at 20 mg mL^{-1} concentrations, overnight heated at 70 °C to dissolve the PS and mixed in the appropriate ratio to achieve the desired host-guest concentration (5 wt%). Films were made and kept in a glovebox and encapsulated using a glass slide and epoxy prior to being measured. The pump and probe originated from a Spectra Physics Solstice Ti:Sapphire laser, outputting pulses of width 80 fs and a repetition rate of 1 kHz at 800 nm. The pump beam was frequency-doubled using a BBO to give 400 nm pulses. Excitation fluence was varied from 9–60 µJcm^{-2} using neutral density filters. The probe beam was generated from the 800 nm fundamental using a noncollinear optical parametric amplifier, built in-house. The probe was further split into a probe and reference, with only the probe beam overlapping with the pump on the sample. The pump-probe delay was controlled using a computer-controlled delay stage. A Hamamatsu G11608-512 InGaAs dual-line array detector was used to measure the transmitted probe and reference.

Computational Details: Gas-phase DFT calculations of HOMO/LUMO of CMAs were carried out by the global hybrid MN15 functional by Truhlar and coworkers[30] in combination with the def2-TZVP basis set by Ahlrichs and coworkers.[31,32] Relativistic effective core potential of 28 and 60 electrons was used to describe the core electrons of Ag and Au, respectively.[33] The ground state was studied by DFT and the excited states by TD-DFT.[34] The employed method provided excited state energies that did not suffer from underestimation typical for TD-DFT,[35,36] as indicated by the recent work on closely related molecules[3,5,21] as well as by earlier comparison to T$_1$ energies calculated by unrestricted DFT for CMA(Au), the unrestricted and TD-DFT T$_1$ energies differing by only 0.004 eV.[8] For the S0 ground state, results using M06 and PBE0 functionals are included for comparison. These calculations were carried out by Gaussian 16.[37] Specific orbital contributions for metal contribution to HOMO and LUMO were calculated by Mulliken population analysis, bond orders were calculated by Mayer bond order analysis using Multiwfn program.[38]

Supporting Information

Supporting Information is available from the Wiley Online Library or from the author.

Acknowledgements

Data Availability Statement

The data set underlying this paper is available at https://doi.org/10.17863/CAM.57427.

Conflict of Interest

The authors declare no conflict of interest.

Keywords

[1] D. Di, A. S. Romanov, L. Yang, J. M. Richter, J. P. H. Rivett, S. Jones, T. H. Thomas, M. A. Jalebi, R. H. Friend, M. Linnolahti, M. Bochmann, D. Credgington, *Science* **2017**, *356*, 159.

[2] P. J. Conaghan, S. M. Menke, A. S. Romanov, S. T. E. Jones, A. J. Pearson, E. W. Evans, M. Bochmann, N. C. Greenham, D. Credgington, *Adv. Mater.* **2018**, *30*, 1802285.

[3] A. S. Romanov, S. T. E. Jones, Q. Gu, P. J. Conaghan, B. H. Drummond, J. Feng, F. Chotard, L. Buizza, M. Foley, M. Linnolahti, D. Credgington, M. Bochmann, *Chem. Sci.* **2019**, *11*, 435.

[4] R. Hamze, S. Shi, S. C. Kapper, D. S. M. Ravinson, L. Estergreen, M. C. Jung, A. C. Tadle, R. Haiges, P. I. Djurovich, J. L. Peltier, R. Jazzar, G. Bertrand, S. E. Bradforth, M. E. Thompson, *J. Am. Chem. Soc.* **2019**, *141*, 8616.

[5] A. S. Romanov, S. T. E. Jones, L. Yang, P. J. Conaghan, D. Di, M. Linnolahti, D. Credgington, M. Bochmann, *Adv. Opt. Mater.* **2018**, *6*, 1801347.

[6] E. J. Taffet, Y. Olivier, F. Lam, D. Beljonne, G. D. C.-M.-A. B. D. Scholes, R. T. L. Rotation, D. D. Fluorescence, *J. Phys. Chem. Lett.* **2018**, *9*, 1620.

[7] R. Hamze, J. L. Peltier, D. Sylvinson, M. Jung, J. Cardenas, R. Haiges, M. Soleilhavoup, R. Jazzar, P. I. Djurovich, G. Bertrand, M. E. Thompson, *Science* **2019**, *363*, 601.

[8] J. Feng, L. Yang, A. S. Romanov, J. Ratanapreechachai, S. T. E. Jones, A.-P. M. Reponen, M. Linnolahti, T. J. H. Hele, A. Köhler, H. Bässler, M. Bochmann, D. Credgington, *Adv. Funct. Mater.* **2020**, *30*, 1908715.

[9] J. Gibson, A. P. Monkman, T. J. Penfold, *ChemPhysChem* **2016**, *17*, 2956.

[10] T. J. Penfold, F. B. Dias, A. P. Monkman, *Chem. Commun.* **2018**, *54*, 3926.

[11] A. Monkman, in *Highly Efficient OLEDs: Materials Based on Thermally Activated. Delayed Fluorescence* (Ed: H. Yersin), Wiley-VCH Verlag GmbH & Co., Weinheim, Germany **2018**, pp. 425–463.

[12] M. K. Etherington, J. Gibson, H. F. Higginbotham, T. J. Penfold, A. P. Monkman, *Nat. Commun.* **2016**, *7*, 13680.

[13] C. R. Hall, A. S. Romanov, M. Bochmann, S. R. Meech, *J. Phys. Chem. Lett.* **2018**, *9*, 5873.

[14] J. Eng, S. Thompson, H. Goodwin, D. Credgington, T. J. Penfold, *Phys. Chem. Chem. Phys.* **2020**, *22*, 4659.

[15] S. Thompson, J. Eng, T. J. Penfold, *J. Chem. Phys.* **2018**, *149*, 014304.

[16] S. Gélinas, O. Paré-Labrosse, C. N. Brosseau, S. Albert-Seifried, C. R. McNeill, K. R. Kirov, I. A. Howard, R. Leonelli, R. H. Friend, C. Silva, *J. Phys. Chem. C* **2011**, *115*, 7114.

[17] A. Rao, P. C. Y. Chow, S. Gélinas, C. W. Schlenker, C. Z. Li, H. L. Yip, A. K. Y. Jen, D. S. Ginger, R. H. Friend, *Nature* **2013**, *500*, 435.

[18] R. D. Burkhart, N. J. Caldwell, G. Haggquist, *J. Photochem. Photobiol., A* **1988**, *45*, 369.

[19] V. Bulović, R. Deshpande, M. E. Thompson, S. R. Forrest, *Chem. Phys. Lett.* **1999**, *308*, 317.

[20] V. Bulović, A. Shoustikov, M. A. Baldo, E. Bose, V. G. Kozlov, M. E. Thompson, S. R. Forrest, *Chem. Phys. Lett.* **1998**, *287*, 455.

[21] A. S. Romanov, L. Yang, S. T. E. Jones, D. Di, O. J. Morley, B. H. Drummond, A. P. M. Reponen, M. Linnolahti, D. Credgington, M. Bochmann, *Chem. Mater.* **2019**, *31*, 3613.

[22] M. A. El-Sayed, *J. Chem. Phys.* **1963**, *38*, 2834.

[23] G. Capano, U. Rothlisberger, I. Tavernelli, T. J. Penfold, *J. Phys. Chem. A* **2015**, *119*, 7026.

[24] T. J. Penfold, E. Gindensperger, C. Daniel, C. M. Marian, *Chem. Rev.* **2018**, *118*, 6975.

[25] H. Uoyama, K. Goushi, K. Shizu, H. Nomura, C. Adachi, *Nature* **2012**, *492*, 234.

[26] Q. Zhang, B. Li, S. Huang, H. Nomura, H. Tanaka, C. Adachi, *Nat. Photonics* **2014**, *8*, 326.

[27] K. Goushi, K. Yoshida, K. Sato, C. Adachi, *Nat. Photonics* **2012**, *6*, 253.

[28] H. Kaji, H. Suzuki, T. Fukushima, K. Shizu, K. Suzuki, S. Kubo, T. Komino, H. Oiwa, F. Suzuki, A. Wakamiya, Y. Murata, C. Adachi, *Nat. Commun.* **2015**, *6*, 8476.

[29] S. Hirata, Y. Sakai, K. Masui, H. Tanaka, S. Y. Lee, H. Nomura, N. Nakamura, M. Yasumatsu, H. Nakanotani, Q. Zhang, K. Shizu, H. Miyazaki, C. Adachi, *Nat. Mater.* **2015**, *14*, 330.

[30] H. S. Yu, X. He, S. L. Li, D. G. Truhlar, *Chem. Sci.* **2016**, *7*, 5032.

[31] F. Weigend, R. Ahlrichs, *Phys. Chem. Chem. Phys.* **2005**, *7*, 3297.

[32] F. Weigend, M. Häser, H. Patzelt, R. Ahlrichs, *Chem. Phys. Lett.* **1998**, *294*, 143.

[33] D. Andrae, U. Häußermann, M. Dolg, H. Stoll, H. Preuß, *Theor. Chim. Acta* **1990**, *77*, 123.

[34] F. Furche, D. Rappoport, M. Olivuccim, *Density Functional Methods for Excited States: Equilibrium Structure and Electronic Spectra in Computational Photochemistry*, Elesvier, Amsterdam **2005**.

[35] A. Dreuw, M. Head-Gordon, *Chem. Rev.* **2005**, *105*, 4009.

[36] B. Moore, H. Sun, N. Govind, K. Kowalski, J. Autschbach, *J. Chem. Theory Comput.* **2015**, *11*, 3305.

[37] M. J. Frisch, G. W. Trucks, H. B. Schlegel, G. E. Scuseria, M. A. Robb, J. R. Cheeseman, *Gaussian 16, Revision A. 03*, Gaussian. Inc., Wallingford CT **2016**.

[38] T. Lu, F. Chen, *J. Comput. Chem.* **2012**, *33*, 580.